Adams, M., Kempka, T., Chabab [Tillner], E., Ziegler, M. (2018): An innovative computationally efficient hydromechanical coupling approach for fault reactivation in geological subsurface utilization. - *Computers and Geosciences*, *111*, pp. 46—57.

DOI: http://doi.org/10.1016/j.cageo.2017.10.007

An innovative computationally efficient hydromechanical coupling approach for fault reactivation in geological subsurface utilization

M. Adams[1,*], T. Kempka[2], E. Chabab[2] & M. Ziegler[1]

[1] Geotechnical Engineering, RWTH Aachen University, Aachen, Mies-van-der-Rohe-Straße 1, 52074 Aachen, Germany

[2] GFZ German Research Centre for Geosciences, Fluid Systems Modelling, Telegrafenberg, 14473 Potsdam, Germany, kempka@gfz-potsdam.de

[*] Corresponding author

E-mail address: adams@geotechnik.rwth-aachen.de
Geotechnical Engineering, RWTH Aachen University, Aachen, Germany
Mies-van-der-Rohe-Straße 1
D – 52074 Aachen
Tel.: +49 241 80 25253

Keywords

Hydromechanical coupling; Semi-analytical coupling; Multiphase fluid flow; Geological faults; Numerical simulation; Subsurface gas storage

Abstract

Estimating the efficiency and sustainability of geological subsurface utilization, i.e., Carbon Capture and Storage (CCS) requires an integrated risk assessment approach, considering the occurring coupled processes, beside others, the potential reactivation of existing faults. In this context, hydraulic and mechanical parameter uncertainties as well as different injection rates have to be considered and quantified to elaborate reliable environmental impact assessments. Consequently, the required sensitivity analyses consume significant computational time due to the high number of realizations that have to be carried out. Due to the high computational costs of two-way coupled simulations in large-scale 3D multiphase fluid flow systems, these are not applicable for the purpose of uncertainty and risk assessments.

Hence, an innovative semi-analytical hydromechanical coupling approach for hydraulic fault reactivation will be introduced. This approach determines the void ratio evolution in representative fault elements using one preliminary base simulation, considering one model geometry and one set of hydromechanical parameters. The void ratio development is then approximated and related to one reference pressure at the base of the fault. The parametrization of the resulting functions is then directly implemented into a multiphase fluid flow simulator to carry out the semi-analytical coupling for the simulation of hydromechanical processes. Hereby, the iterative parameter exchange between the multiphase and mechanical simulators is omitted, since the update of porosity and permeability is controlled by one reference pore pressure at the fault base. The suggested procedure is capable to reduce the computational time required by coupled hydromechanical simulations of a multitude of injection rates by a factor of up to 15.

1. Introduction

For the simulation of hydromechanical multiphase fluid flow processes in reservoirs, i.e., Carbon Capture and Storage (CCS), numerical modelling is state of the art (Altmann et al., 2014; Cappa and Rutqvist, 2011; Kempka and Kühn, 2013; Rutqvist and Tsang, 2002; Rutqvist et al., 2007, 2008; Rutqvist, 2010). For that purpose, hydraulic multiphase flow and geomechanical simulators are sequentially coupled using one-way or two-way approaches (Settari and Mourits, 1994; Settari et al., 2005; Settari, 2012; Kempka et al., 2014, 2015; Tillner et al., 2014; Walters et al., 2002).

For a one-way coupling, parameters like liquid phase pressure P_l, gas phase pressure P_g, and liquid saturation S_l have to be determined using a multiphase flow simulator. After converting these data into an average pore pressure P following Eq. 1

$$P = S_l \cdot P_l + (1 - S_l)\ P_g, \qquad (1)$$

P is transferred to the geomechanical simulator. An additional coupling parameter for non-isothermal studies is the temperature T. If this data transfer is occurring only in one direction (one-way), the resulting volumetric strain ε_V will not be fed back to the multiphase flow simulator for updating porosity and permeability (Fig. 1 (a)). In case of large volumetric strains ε_V occurring during the simulation, a one-way coupling may lead to inaccurate results (Cappa and Rutqvist, 2011; Chabab and Kempka, 2016; Langhi et al., 2010; Lautenschläger et al., 2013; Righetto et al., 2013; Zhang et al., 2011). A method to consider large volumetric strains comprises the use of sequentially two-way coupled simulations, where the coupling parameters P, intrinsic permeability k and porosity ϕ are transferred in both directions (two-way) between the simulators. Hence, porosity and permeability are updated iteratively during the entire simulation cycle (Fig. 1 (b)) and considered in the hydraulic simulator.

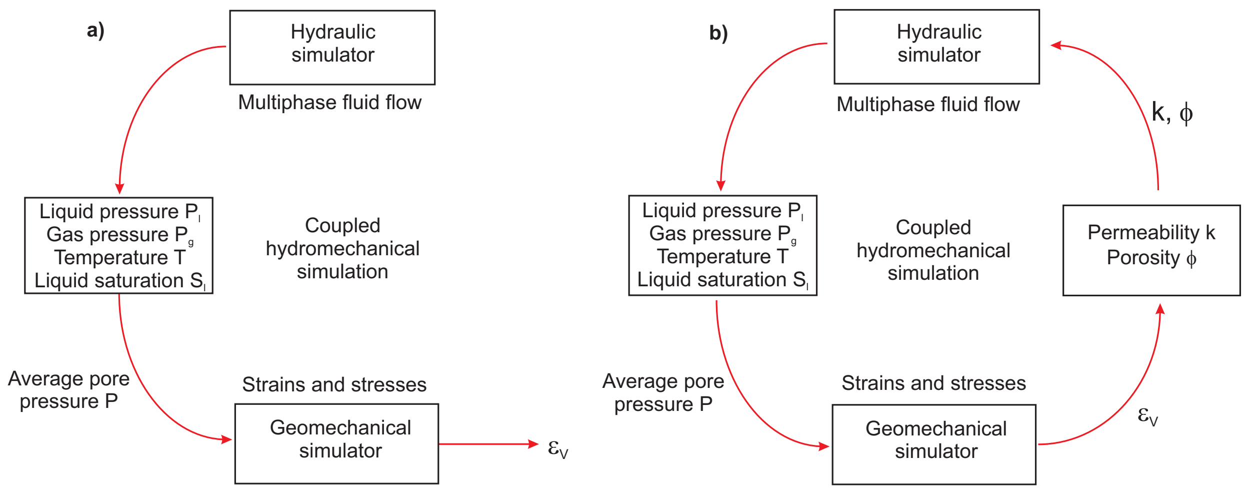

Fig. 1 Types of sequential coupling: (a) One-way coupling (no update of porosity and permeability) and (b) Two-way coupling (with update of porosity and permeability).

To estimate the efficiency and sustainability of geological subsurface utilization, uncertainty and risk assessments considering the occurring coupled processes, i.e., the potential reactivation of existing faults, are mandatory. For reliable environmental impact assessments, hydraulic and mechanical parameter uncertainties, with their consideration would extending beyond the scope of the present study, as well as the injection rate of the fluid or gas have to be considered and quantified by a representatively high number of computational realizations. Consequently, the required sensitivity analyses consume significant computational time. Due to the high computational demand of sequentially two-way coupled simulations in large-scale 3D simulations, these are not applicable for the purpose of risk assessments. Hence, an innovative approach for a hydromechanical two-way coupling to assess hydraulic fault reactivation, based on a semi-analytical coupling is introduced in the following.

Parameterizing the semi-analytical approach, using the mechanical response of a one-way coupled single-phase fluid flow simulation and implementing it directly into a multiphase fluid flow simulator, enables us to omit the iterative parameter exchange between the hydraulic and the mechanical simulators, whereby permeability and porosity updates are controlled analytically. Under validity of the hypothesis that during the CO_2 injection period, the hydromechanical behavior of geological faults is predominantly controlled by the brine properties, we implement and discuss a semi-analytical approach in Section 2.1. For its general validation, we present and discuss the results of three parametric studies of single-phase fluid flow simulations carried out with Abaqus® (Abaqus, 2010) in Section 2.2. Finally, a validation of our hypothesis for coupled hydromechanical simulations involving multiphase fluid flow by comparing semi-analytically coupled simulation results against those of our benchmark simulations, carried out as sequentially two-way coupled hydromechanical simulations with multiphase fluid flow, and established by using a coupling between the TOUGH2-MP/ECO$_2$N and FLAC^{3D} simulators (Cappa and Rutqvist, 2011; Itasca, 2013; Rutqvist et al., 2007; Pruess, 2005; Zhang et al., 2008) is discussed in Section 3.

2. Implementation and validation of the semi-analytical coupling approach considering single phase fluid flow

To reduce the computational time for two-way coupled simulations a methodology to decouple the hydraulic and geomechanical simulators is introduced in this study.

2.1 Description of the approach and derivation of its parametrization

In one-way and two-way coupled simulations, the presence of a gaseous phase is only indirectly considered by updating P at each time step (Equation 1), as the average pore pressure P is the hydraulic coupling parameter between the multiphase flow and the geomechanical simulations. Generally, the presence or absence of a gas phase, i.e., CO_2 influences the average pore pressure P determined in the multiphase fluid flow simulator due to gas compressibility, viscosity and the occurrence of capillary pressures. Conceptually, CO_2 storage reservoirs are generally located in geological anticline structures to benefit from structural and stratigraphic trapping mechanisms. Furthermore, average fluid flow velocities of brine and gaseous CO_2 amount to only a few meters per year (Holloway 2005; IPCC 2005). Hence, the migration of the CO_2-rich phase in a reservoir proceeds over a relatively long time period. Both mechanisms are suitable to avoid uncontrolled CO_2 migration towards known geological faults in the injection well near- and far-field. Anyhow, before CO_2 can flow through hydraulically reactivated faults, it has to displace the brine in the reservoir and in a present hydraulically conductive fault. This is accompanied by a pore pressure increase, and hence decreasing effective stresses. Until leaking CO_2 reaches the upper fault region and possibly enters a shallower aquifer, the pore pressure increase inside the fault is predominantly controlled by the fluid properties of brine (Cappa and Rutqvist, 2011; Birkholzer et al., 2009; Tillner et al., 2013). Hence, in our approach we make the assumption that during this process, the analytical functions for updating the fault's permeability and porosity can be sufficiently calibrated and parametrized by a single phase fluid flow base simulation, as discussed in Section 3.

Fig. 2 shows the general workflow of the semi-analytical coupling approach. In a first step, a single one-way coupled base simulation, indicated by the green box is carried out for one model geometry and one set of hydromechanical parameters to estimate the void ratio evolution in representative fault elements and the pore pressure distribution of one reference element.

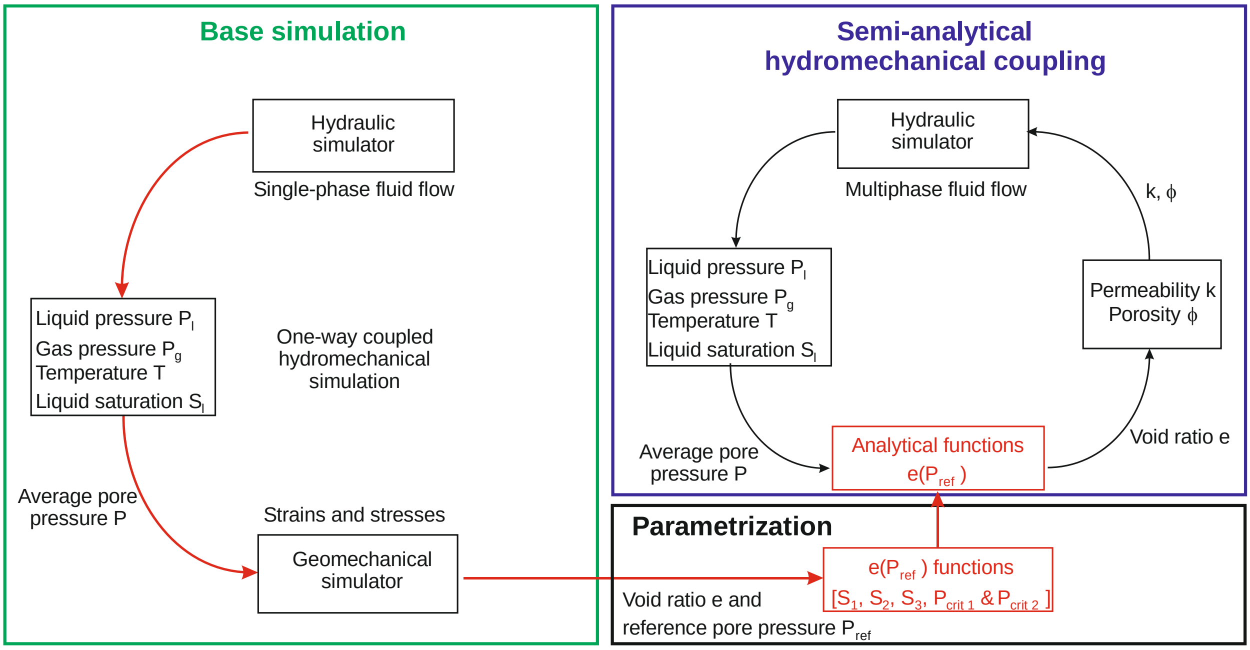

Fig. 2 General workflow of the semi-analytical hydromechanical coupling scheme. Based on a one-way coupled single-phase fluid flow base simulation, $e(P_{ref})$ functions (void ratio e over reference pore pressure P_{Ref} are generated (red box). These functions are directly implemented into a multiphase fluid flow simulator to control the update of porosity and permeability of the fault zone, since the geomechanical simulator is omitted in the suggested approach.

Changing stress states of shallower fault elements, potentially resulting in fault reactivation, can result from pore pressure increases within these elements as well as from a stress relocation from deeper located and already plastified elements. Hence, we relate the void ratio evolutions e of all observation points to a single reference pressure P_{ref}, to address both cases. While the observation points representing the mechanical behavior of adjacent element groups are located in the fault damage zone (Points 1 to 6 in Fig. 4), P_{ref} is located at the intersection between the fault and the storage reservoir.

Within our studies, we recognized that elements experiencing a similar amount of void ratio increase during fault reactivation are distributed over a large fault region. As a consequence, the distance between two observation points can be set in maximum to 200 m to partition the homogeneous fault in our study. In case of a heterogeneous hydraulic parameter distribution on the fault plane, additional observation points are required.

The analytical $e(P_{ref})$ functions (red box in Fig. 2) are generated and parametrized (black box in Fig. 2) on the basis of the results of a single fluid flow base simulation. As the pore pressure distribution is driven by the Darcy velocity and a pressure gradient, the constant hydraulic conductivity in one-way coupled simulations leads to linear void ratio-to-pore pressure relations, while we recognize nonlinear behavior in two-way coupled simulations. Thus, the $e(P_{ref})$ functions of one-way coupled simulations can be sufficiently linearized, which will be demonstrated in Section 2.2.2 on the basis of the simulation results of parametric studies 1 and 2 presented in Table 1, providing an overview of the simulations discussed in the scope of this study.

These 35 simulations are organized in three parametric studies, where studies 1 and 2 aim at investigation of the hydromechanical behavior of fault zones in one-way coupled simulations, considering varying injection regimes and initial fault permeabilities. Study 3 considers one-way, two-way and semi-analytically coupled simulations to validate the new coupling approach.

Table 1 Studies undertaken to show that $e(P_{ref})$ functions show an invariant behavior towards the injection rate (study 1), that α_1, α_2 and α_3 are invariant towards the initial fault permeability (study 2) and to validate the semi-analytical hydromechanical coupling approach (study 3).

Study 1: Invariant behavior of $e(P_{ref})$ towards the injection rate			
Scenario	Permeability k [m²]	Injection rate [kg/s/m]	H-M coupling method
S1	5 x 10^{-16}	0.0018	one-way
S2	5 x 10^{-16}	0.0023	one-way
S3	5 x 10^{-16}	0.0027	one-way
S4	5 x 10^{-16}	0.0032	one-way
S5	5 x 10^{-15}	0.0018	one-way
S6	5 x 10^{-15}	0.0023	one-way
S7	5 x 10^{-15}	0.0027	one-way
S8	5 x 10^{-15}	0.0032	one-way
Study 2: Invariant behavior of α_1, α_2 and α_3 towards the initial fault permeability			
S9	2.5 x 10^{-16}	0.0027	one-way
S10	5 x 10^{-16}	0.0027	one-way
S11	7.5 x 10^{-16}	0.0027	one-way
S12	1 x 10^{-15}	0.0027	one-way
S13	2.5 x 10^{-15}	0.0027	one-way
S14	5 x 10^{-15}	0.0027	one-way
S15	7.5 x 10^{-15}	0.0027	one-way
S16	1 x 10^{-14}	0.0027	one-way
S17	2.5 x 10^{-14}	0.0027	one-way

Study 3: Validation of the semi-analytical coupling approach			
Scenario	Permeability k [m²]	Injection rate [kg/s/m]	H-M coupling method
S18	5 x 10^{-16}	0.0027	one-way
S19	1 x 10^{-16}	0.0018	two-way
S20	1 x 10^{-16}	0.0023	two-way
S21	1 x 10^{-16}	0.0027	two-way
S22	1 x 10^{-16}	0.0032	two-way
S23	1 x 10^{-16}	0.0018	semi-analytical
S24	1 x 10^{-16}	0.0023	semi-analytical
S25	1 x 10^{-16}	0.0027	semi-analytical
S26	1 x 10^{-16}	0.0032	semi-analytical
S27	5 x 10^{-15}	0.0027	one-way
S28	1 x 10^{-15}	0.0018	two-way
S29	1 x 10^{-15}	0.0023	two-way
S30	1 x 10^{-15}	0.0027	two-way
S31	1 x 10^{-15}	0.0032	two-way
S32	1 x 10^{-15}	0.0018	semi-analytical
S33	1 x 10^{-15}	0.0023	semi-analytical
S34	1 x 10^{-15}	0.0027	semi-analytical
S35	1 x 10^{-15}	0.0032	semi-analytical

Exemplarily for all others, Fig. 3 shows the $e(P_{ref})$ function (blue solid line) for Point 3 of Scenario S18 to introduce the linearization (red dashed line) and parametrization of the one-way coupled single-phase fluid flow base simulations, used to determine the analytical functions applied for the semi-analytical coupling approach. For the determination of these parameters, the length of one percent void ratio evolution has to be scaled to 1 MPa P_{ref} in general.

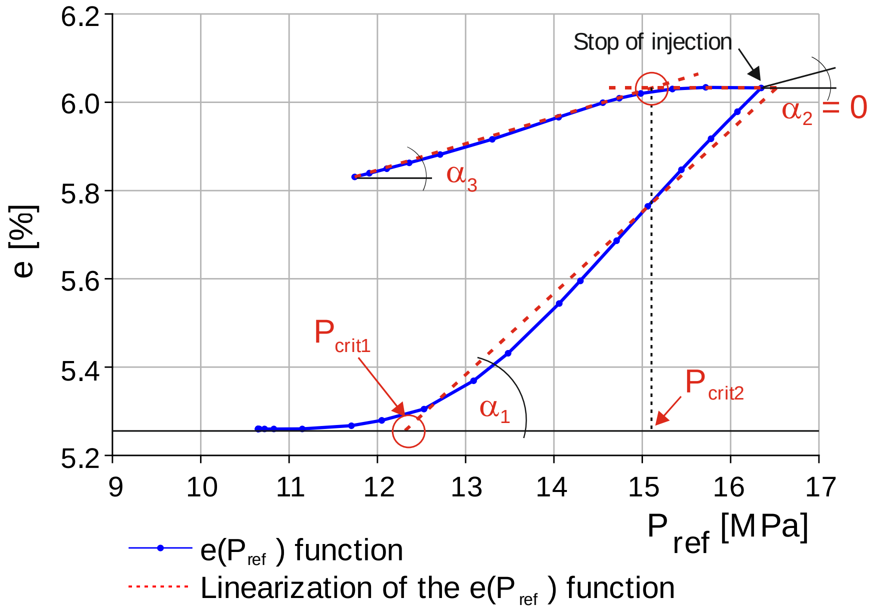

Fig. 3 Linearization and parametrization of the semi-analytical hydromechanical coupling approach, applying the e(P_{ref}) function of a one-way coupled simulation, using a five times higher initial fault permeability and introducing the inclinations α_1, α_2 and α_3 and two pore pressure control points P_{crit1} and P_{crit2}. Note that the lengths of 0.2 percent void ratio evolution are scaled to 1 MPa P_{ref} to improve visibility.

We identify a first control pore pressure P_{crit1} at the intersection of the red-dashed line inclined at the angle α_1 and the parallel to the x-axis at the level of the initial void ratio (5.263 %), indicating the occurrence of increasing volumetric strain/void ratio prevalently induced by shear failure accompanied with plastic deformation in the corresponding fault group. Hence, the update of permeability and porosity starts, when P_{ref} in the reference element exceeds the P_{crit1} value, and is controlled by the three inclinations α_1, α_2 and α_3, which operate as a stiffness to control the void ratio evolution. In this context, α_1 represents the void ratio evolution during the injection period predominantly induced by plastic deformations, while α_2 and α_3 apply for the post-injection period characterized by elastic deformations only. Furthermore, a second control pore pressure P_{crit2} is introduced at the intersection of the lines inclined at α_2 and α_3, which acts as transition parameter between the two straight lines. The sectionalized linearization of α_1 is approximated by the method of least squares, α_2 and α_3 by tangents touching the two parts of the curves representing the post-injection period. The transition point between α_1 and α_2 is variable and represents the maximum pore pressure depending on the fluid injection history of the reservoir.

The semi-analytical parametrization (α_1, α_2, α_3, $P_{crit\,1}$ and $P_{crit\,2}$) used for the semi-analytical simulations, considering initial fault permeabilities of $k = 10^{-16}$ m² and $k = 10^{-15}$ m² (Section 2.2.2) to validate the new approach is given in Table 2 and Table 3. Furthermore, the average depth at each observation point (Points 1 to 6) is provided.

Table 2 Parametrization used for the semi-analytically coupled simulation runs with $k_{ini} = 10^{-16}$ m².

		Linearized inclinations of $e(P_{ref})$ functions			Pore pressure control points in the reference cell (P_{ref}) [MPa]	
Point	Depth [m]	α_1 [°]	α_2 [°]	α_3 [°]	$P_{crit\,1}$	$P_{crit\,2}$
1	570.3	7.2	0.0	1.2	13.3	14.8
2	695.3	10.2	0.0	2.5	13.1	14.9
3	820.3	11.9	0.0	3.4	12.6	15.3
4	945.3	12.5	1.1	3.7	12.3	15.6
5	1012.5	12.2	2.0	3.7	12.2	15.7
6	1160.0	13.0	0.0	4.6	12.4	15.5

Table 3 Parametrization used for the semi-analytically coupled simulation runs with $k_{ini} = 10^{-15}$ m².

		Linearized inclinations of $e(P_{ref})$ functions			Pore pressure control points in the reference cell (P_{ref}) [MPa]	
Point	Depth [m]	α_1 [°]	α_2 [°]	α_3 [°]	$P_{crit\,1}$	$P_{crit\,2}$
1	570.3	6.1	0.2	1.1	11.9	14.0
2	695.3	8.4	0.5	2.1	11.7	14.0
3	820.3	10.5	1.4	3.1	11.5	14.0
4	945.3	10.9	3.7	3.7	11.4	14.0
5	1012.5	10.7	3.6	3.6	11.3	14.1
6	1160.0	10.8	2.1	4.2	11.4	14.1

As one base simulation can be employed to investigate the impact of a multitude of different injection rates, the invariant behavior of the semi-analytical parametrization related to the injection rates is required and is validated by the results of parametric study 1 (Table 1). In addition, the results of study 2 are used to demonstrate that the parameters α_1, α_2 and α_3 show invariant behavior related to the initial fault permeability. This allows us to demonstrate that the nonlinear shape of the $e(P_{ref})$ functions, generated with two-way coupled simulations can be sufficiently approximated by one-way coupled simulations. Therefore, $p_{crit\ 1}$ has to be shifted to a lower value, which is realized by generally employing a fault permeability multiplier of 5 in the base simulation to estimate the $e(P_{ref})$ function used for the parameterization of the semi-analytically coupled simulations. This permeability multiplier is only applied in the base simulation, while the semi-analytically coupled simulations of course consider the initial fault permeability. A detailed explanation of this general permeability multiplier is given in Section 2.2.2.

Finally, these functions are implemented into the semi-analytical coupling approach as shown in the blue box in Fig. 2. The coupling approach operates in a semi-analytical manner, whereby the averaged pore pressures P are determined numerically by the multiphase flow simulator during the simulation run, whereas permeability k and porosity ϕ updates are directly managed by a set of functions representing the void ratio evolution determined at observation points. Hence, the iterative parameter exchange between both simulators is omitted.

Further, permeability and porosity updates are undertaken for the geological fault only, implying that reservoir and caprock integrity are not compromised by the induced pore pressure increase. To overcome this restriction into our approach, we suggest to assign elasto-plastic material behavior for the surrounding rocks to parametrize the base simulation. In consequence, only the results of the base simulations are suitable for parameterization, exhibiting that pore pressure increase does not compromise the integrity of the surrounding rocks. Considering the limitation of one base simulation being valid for a specific model geometry and one set of hydromechanical parameters, the suggested procedure is capable to significantly reduce the computational time required by coupled hydromechanical simulations of a multitude of injection rates.

2.2 Validation of the semi-analytical coupling approach

2.2.1 Setup of the synthetic model

To validate the semi-analytical coupling approach for single phase fluid flow, 35 simulation runs organized in three parametric studies shown in Table 1, considering a synthetic 2D model plotted in Fig. 4 were undertaken as described in Adams et al., 2015 and are discussed in detail in Section 2.2.2. The top of the 20-m thick reservoir formation is located at 1,000 m depth and an aquifer with a thickness of 500 m is implemented at the model top. Caprock formations are present above and below the reservoir, cut by a fault dipping by 70° in 500 m distance from the injection well (injection rates are given in Table 1). As it is not possible to differentiate between fault cores and damage zones within large-scale models, we apply a lumped fault permeability as previously introduced by Cappa and Rutqvist (2011). The fault is partitioned into six element groups, with one element representing each group (Points 1 to 6, black squares in Fig. 4). Additionally, one single element is defined as reference element at the transition between the fault and reservoir to derive the reference pore pressure P_{ref} for the parametrization of the semi-analytical hydromechanical coupling (red square in Fig. 4).We simulated a 20-year injection and a 30-year post-injection period of brine (salinity of 20 % NaCl by weight) to maintain a simulation setup not potentially compromised by multiphase flow effects. In Section 3, this generalization is validated for multiphase fluid flow, and we demonstrate that our coupling approach is capable to handle multiphase flow effects in the presence of a gas phase.

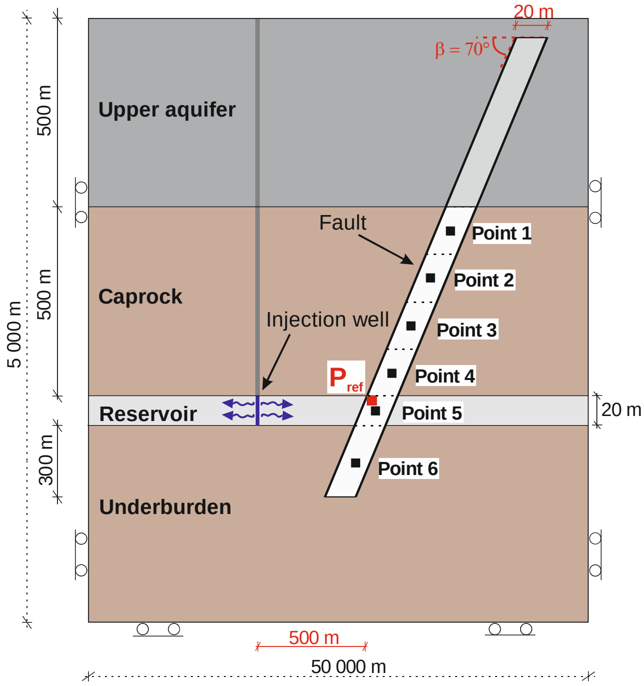

Fig. 4 Schematic overview of the synthetic model considering a 20 m wide fault with a dip of β = 70° as applied for the implementation of the semi-analytical coupling methodology, based on single-phase fluid flow simulations.

The finite element program Abaqus® is used, assuming a 50 km wide and 5 km thick model, plane-strain conditions and an extensional stress regime with σ_h / σ_v = 0.7 (total horizontal to vertical stresses). Considering a hydrostatic pressure gradient, atmospheric pressure at the ground surface and salinity in all formations according to the information given in Table 4, the initial fluid pressure at the top of the reservoir amounts to 10.62 MPa. Temperature distribution is calculated using a geothermal gradient of 30 °C/km, resulting in an average temperature of 40 °C in the reservoir. Isothermal conditions are assumed for all simulation runs. Reservoir rock behavior is considered to be elastic for simplicity, whereas the fault zone follows a linear and ideal elastoplastic constitutive behavior based on the Mohr-Coulomb failure criterion (Altmann et al., 2014; Langhi et al., 2010; Mandl, 1988; Nguyen et al., 2016; Orlic, 2016; Pan et al., 2016; Rutqvist et al., 2016; Verdon and Stork, 2016; Vilarrasa et al, 2016; Zhang et al., 2009, 2010, 2011, 2013, 2015). The initial permeability of the fault is varied between k = 1 x 10^{-16} m² and k = 2.5 x 10^{-14} m². All further material properties, e.g., dry specific weight γ_d, Young's modulus E, Poisson's ratio ν, friction angle

φ, cohesion c, dilation angle ψ, porosity ϕ, permeability k for each formation used in the simulations are given in Table 4. Besides the initial permeability and porosity, the given material properties are valid for the entire fault zone. Hereby, porosity and permeability of the upper part of the fault (50 m to 500 m depth) are equal to those of the upper aquifer.

In all simulations presented here, porosity and permeability are updated according to Chin et al., 2000 using Equations (2) and (3)

$$\phi = 1 - \left(1 - \phi_i\right)e^{-\varepsilon v} \quad (2)$$

$$k = k_i \left(\frac{\phi}{\phi_i}\right)^n. \quad (3)$$

Here, ϕ is the porosity at a given volumetric strain, ϕ_i the initial porosity, ε_v the volumetric strain increment, k the permeability at a given strain, k_i the initial permeability, and n a porosity sensitivity exponent. In the present study, n is set to 10 to achieve a fault permeability increase by about one magnitude (Cappa and Rutqvist, 2011) for a maximum volumetric strain of 1.5 %. Brine and CO_2 fluid data are derived from Battistelli et al., 1997 and Spycher et al., 2003.

Table 4 Material properties used to simulate single-phase fluid flow in the reservoir-caprock system with one fault.

Parameters	Reference	Reservoir	Caprock	Underbur-den	Upper aquifer	Fault
Young's modulus, E (GPa)	Cappa and Rutqvist, 2011	10	10	10	10	1
Poisson's ratio, ν (-)	Cappa and Rutqvist, 2011	0.25	0.25	0.25	0.25	0.25
Rock density, ρ_s (kg/m^3)	Cappa and Rutqvist, 2011	2 260	2 260	2 260	2 260	2 260
Biot's coefficient, α (-)	Cappa and Rutqvist, 2011	1	1	1	1	1
Friction angle, φ (◦)	Cappa and Rutqvist, 2011	-	-	-	-	25
Dilation angle, ψ (◦)	Cappa and Rutqvist, 2011	-	-	-	-	20
Porosity, ϕ (-)	Cappa and Rutqvist, 2011	0.1	0.01	0.01	0.1	0.05
Permeability, k (m^2)	Cappa and Rutqvist, 2011	10^{-13}	10^{-19}	10^{-19}	10^{-14}	-
Salinity (% NaCl by weight)	Assumed	20	15	20	10	15

2.2.2 Results and discussion

The influence of varying initial intrinsic fault permeability and injection rate on the fault's void ratio evolution was investigated in three parametric studies (S1 – S8, S9 – S17 and S18 – S35) given in Table 1. The first and the second study were run in an one-way coupled manner, while the third one was employed to validate the coupling approach by a comparison of the pore pressure distribution determined by the two-way and semi-analytically coupled simulations.

Fig. 5 shows the $e(P_{ref})$ functions of all six observation points determined in one-way coupled simulations, considering four different injection rates (S5 – S8) and an initial fault permeability of 5×10^{-15} m^2. As all void ratio evolutions of one simulation run are related to one reference pore pressure, all six curves show the same maximum pore pressure, i.e., 13 MPa for the lowest (blue curve) and 14.8 MPa for the highest injection rate (black curve). Linearizing and parametrizing these curves according to Fig. 3, we observe decreasing maximum void ratio evolutions for shallower observation points, which lead to six different parameter sets describing the semi-analytical coupling, i.e, $\alpha_{1,\, Pnt\, 1}$ to $\alpha_{1,\, Pnt\, 6}$ and $P_{crit\, 1,\, Pnt\, 1}$ to $P_{crit\, 1,\, Pnt\, 6}$ in Fig. 5.

As we recognize for each injection rate identical values for α_1, α_2, α_3 and P_{crit1} in each observation point, we emphasize that the calibration and parametrization of the semi-analytical coupling is injection rate-independent. Opposite to this, Fig. 5 shows an injection rate-dependent behavior for P_{crit2}: the higher the injection rate, the higher P_{crit2}. In hydromechanically coupled simulations, porosity and permeability updates are undertaken based on the results calculated in the prior simulation step and remain constant during the subsequent one. As a consequence, a constant void ratio is automatically considered by the semi-analytical coupling approach. Furthermore, we recognize a fast pore pressure decrease by more than 1 MPa within the first days in the reservoir and the fault after the injection stop, what emphasizes the short time period for which the inclination α_2 is valid. Hence, we consider the non-invariant behavior of $p_{crit\, 2}$ related to different injection rates to have negligible influence on the results of the semi-analytical coupling only.

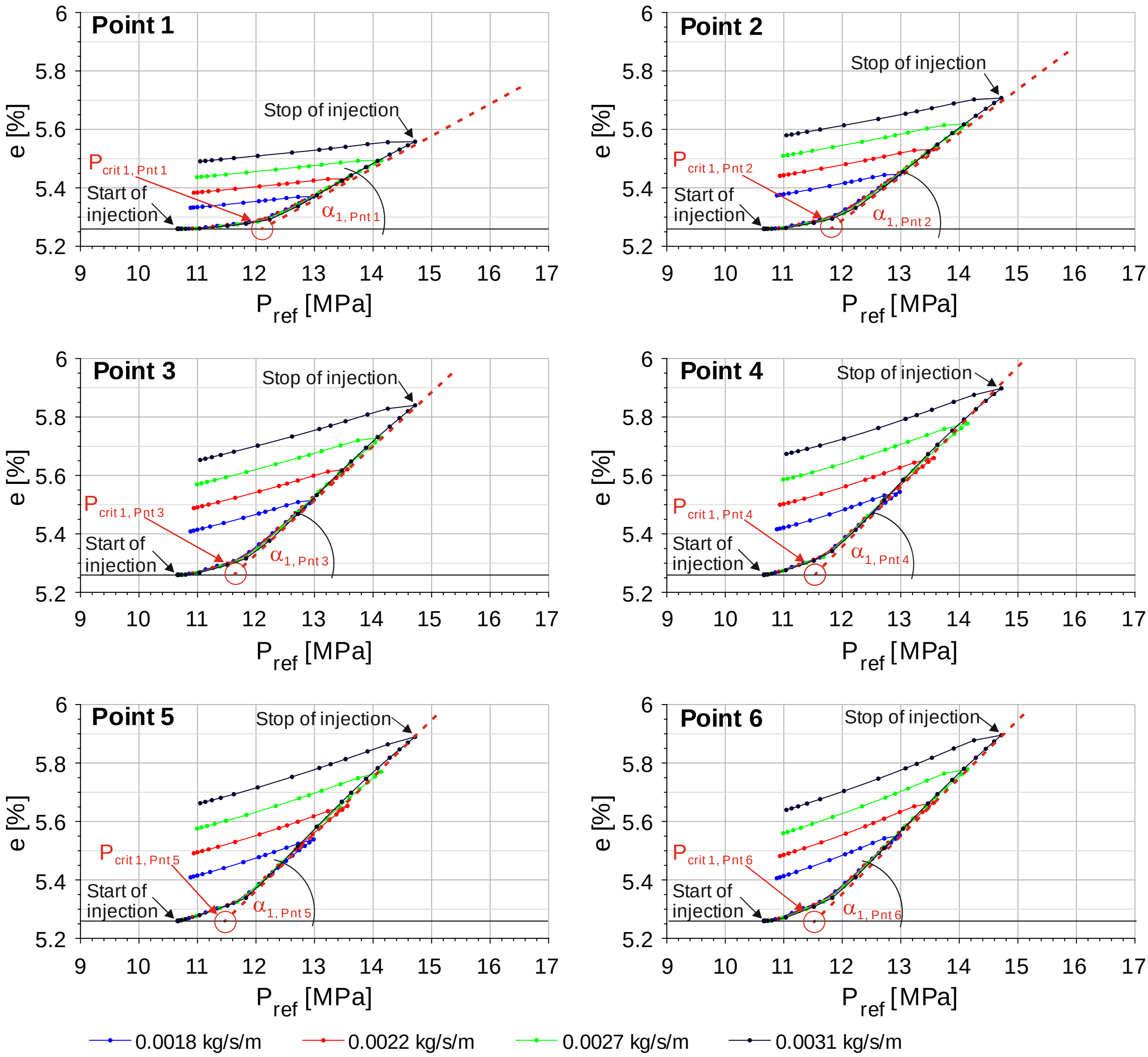

Fig. 5 Diagrams of e(P_{ref}) functions of one-way coupled simulations, considering the same initial permeability and four different injection rates (scenarios S5 – S8) occurring at all observation points (Points 1-6). These functions show the same inclinations α_1, α_2 and α_3 and P_{crit1} for each injection rate. Hence, the calibration and parametrization of the semi-analytical coupling approach is independent from the injection rate used in the base simulation.

Representative for all other curves, the e(P_{ref}) curves at Point 3, considering one-way coupling, a constant injection rate of 0.0027 kg/s/m and varying initial fault permeabilities between 2.5 x 10^{-16} and 2.5 x 10^{-14} m² are shown in Fig. 6. Linearizing these e(P_{ref}) functions (red dashed lines) illustrates that also this parameter setup leads to identical inclinations α_1, α_2 and α_3 as for Point 3 in Fig. 5. Furthermore, we identify decreasing $P_{crit\ 1}$ values accompanied by increasing initial fault permeabilities, converging against 11.4 MPa for permeabilities smaller/equal than 2.5 x 10^{-15} m².

The residual initial permeabilities result in $P_{crit\ 1}$ values between 11.4 MPa and 12.9 MPa. Hence, varying initial permeabilities only shift the e(P_{ref}) functions controlled by $P_{crit\ 1}$, but do not affect the inclinations α_1 to α_3.

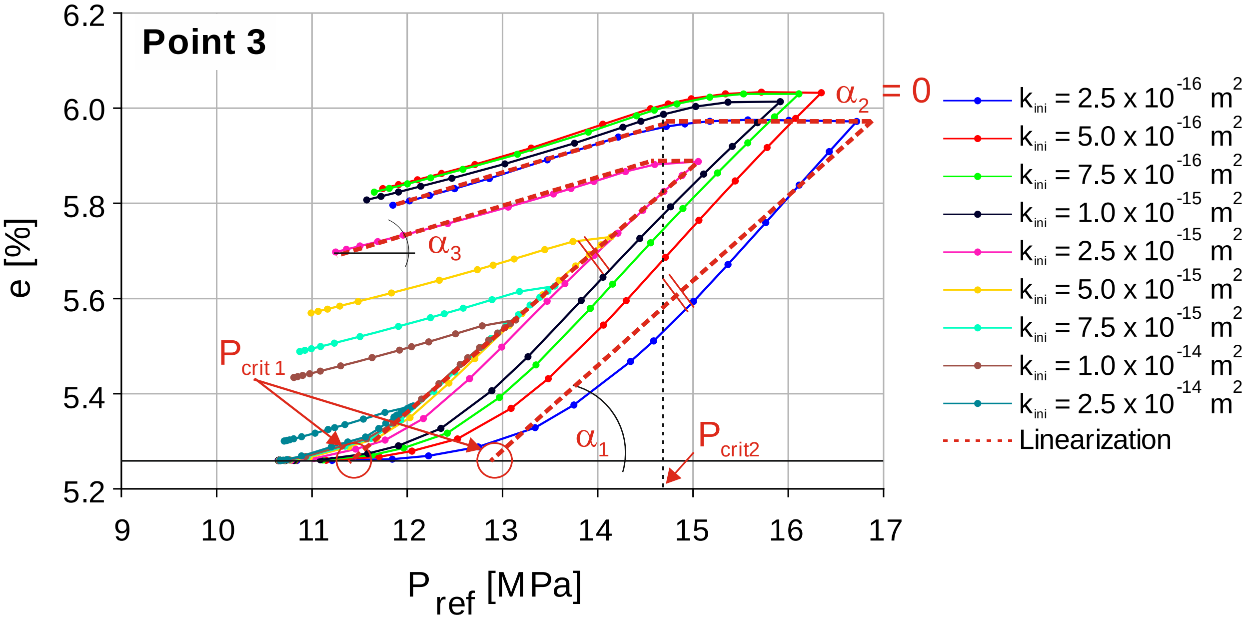

Fig. 6 Nine e(P_{ref}) functions determined by one-way coupled base simulations, considering an injection rate of 0.0027 kg/s/m and varying initial fault permeabilities between 2.5 x 10^{-16} and 2.5 x 10^{-14} m^2 show equal inclinations α_1 to α_3 and a shift of the linearized functions controlled by $P_{crit\ 1}$.

Due to the update of porosity and permeability, the results of two-way coupled simulations, considering four different injection rates and an initial fault permeability of k = 10^{-16} m^2 (Fig. 7, black and grey shaded lines) show a nonlinear relationship between void ratio evolution and P_{ref}, increasing with higher injection rates. Additionally, the linearized run of one-way coupled e(P_{ref}) functions (dashed blue and red lines in Fig. 7), considering initial fault permeabilities specifically higher (k = 2.5 and 5.0 x 10^{-16} m^2) show that the nonlinear behavior of two-way coupled simulations can be approximated by the one-way coupled base simulations. At the intersection between the linearized e(P_{ref}) functions and the two-way coupled e(P_{ref}) functions (green points in Fig. 7), a boundary between two different sections is introduced.

Hence, that approximation method generally overestimates the void ratio evolution at the beginning of the update and underestimates it at the end of the injection period (section right to the green points in Fig. 7). This goes along with a better fit of the one-way coupled base simulation using a permeability multiplier of 2.5 (blue line) in the section left of the point of intersection with the grey e(P_{ref}) function (green point in Fig. 7), while the use of a permeability multiplier of 5.0 (red line) provides an improved approximation of the section right to the intersection. However, as the permeability update used in this paper (Chin et al., 2000) is driven by a power law exponent (see Equations (2) and (3)), a good approximation of the section right to the intersection is more relevant.

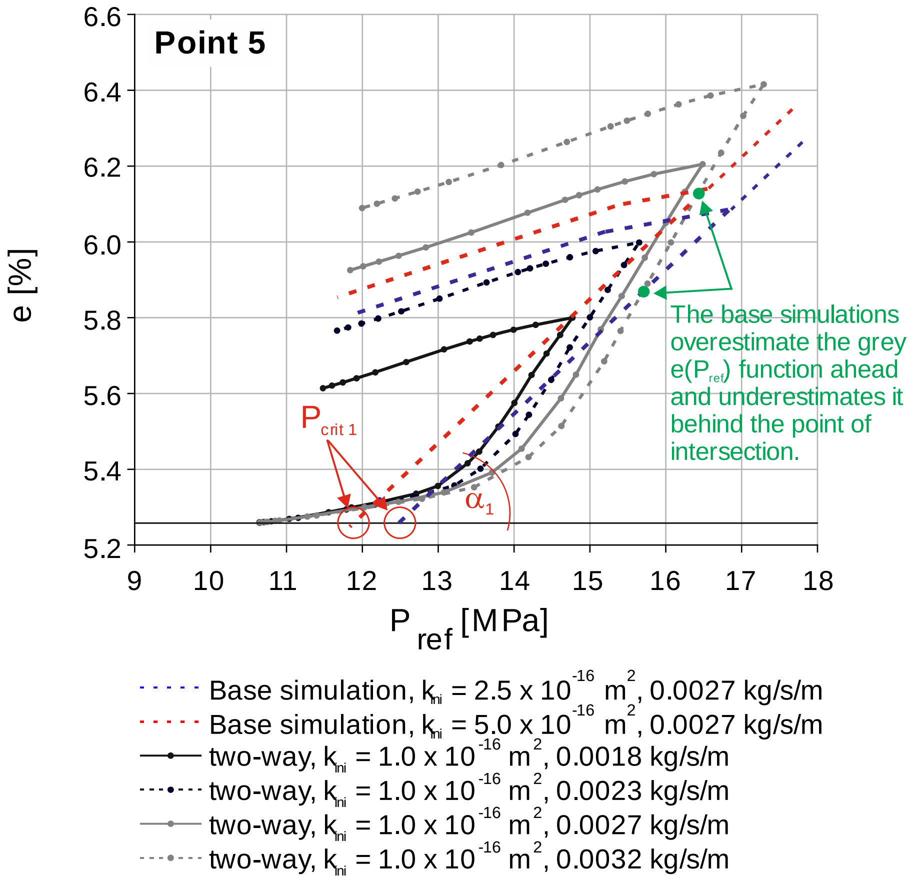

Fig. 7 e(P_{ref}) functions show the nonlinear behavior of four two-way coupled simulations. The nonlinearity increases with increasing injection rates. The linearized run of two base simulations (blue and red dashed lines), considering k_{ini} = 2.5 x 10^{-16} and k_{ini} = 5 x 10^{-16} m^2 can sufficiently approximate the e(P_{ref}) functions of two-way coupled simulations.

Additionally, the approximation of the $e(P_{ref})$ curves by the semi-analytical parametrization considering a permeability multiplier of 5.0 shows higher coefficients of approximation compared to the parametrization considering a multiplier of 2.5.

In an additional parametric study which is not discussed in detail in here, we investigated the influence of different sensitivity exponents n for deriving permeability from porosity (Equation 3) in two-way coupled simulations. Considering n values between 10 and 20 as well as an injection rate of 0.0027 kg/s/m, we identified flattening pore pressure increases in the fault and reservoir elements with increasing sensitivity exponents, accompanied by lower void ratio increases. In addition, we recognized that the parameters α_1, α_2, α_3 and $P_{crit\ 1}$ are identical for all exponent variations. Since higher exponents result in higher permeabilities for the same porosity increase, this corresponds with higher hydraulic conductivities resulting in lower pore pressure increases. Hence, we state that an upper limit for pore pressure increases exists, while the parametrization of the semi-analytical approach is invariant with respect to the rate of fault permeability increase.

In combination with the results of the aforementioned studies, i.e., convergence of $P_{crit\ 1}$ against a fix value for initial permeabilities less than or equal to 2.5×10^{-15} m² (Fig. 6) and the discussion of the results shown in Fig. 7, we generally recommend to use an initial fault permeability five times higher than that in the two-way coupled simulations to parameterize the semi-analytical approach by one base simulation. Furthermore, these general perceptions, i.e., injection rate-independent parametrization and linear void ratio-over-reference pore pressure behavior for one-way coupled simulations point out the general validity of the suggested approach.

Finally, the semi-analytical coupling approach is validated by a comparison of pore pressure distributions over time, resulting from four different brine injection rates given in Table 1. Based on two single base simulations (S18 and S27) considering an initial permeability five times higher than that applied in the benchmark simulations (10^{-15} and 10^{-16} m²), the parametrization for the semi-analytical coupling method is given in Table 2 and Table 3. A comparison of pore pressure distributions over time between the semi-analytically (red dashed lines) and two-way coupled (blue solid lines) simulations is given in Fig. 8 and Fig. 9 for all observation points. Maximum reference pore pressure P_{ref} increases by 4.12 MPa for the lowest and by 6.64 MPa for the highest injection rate are observed. For all investigated scenarios, we achieve a remarkably good agreement between the validation (semi-analytical) and benchmark simulation (two-way) results.

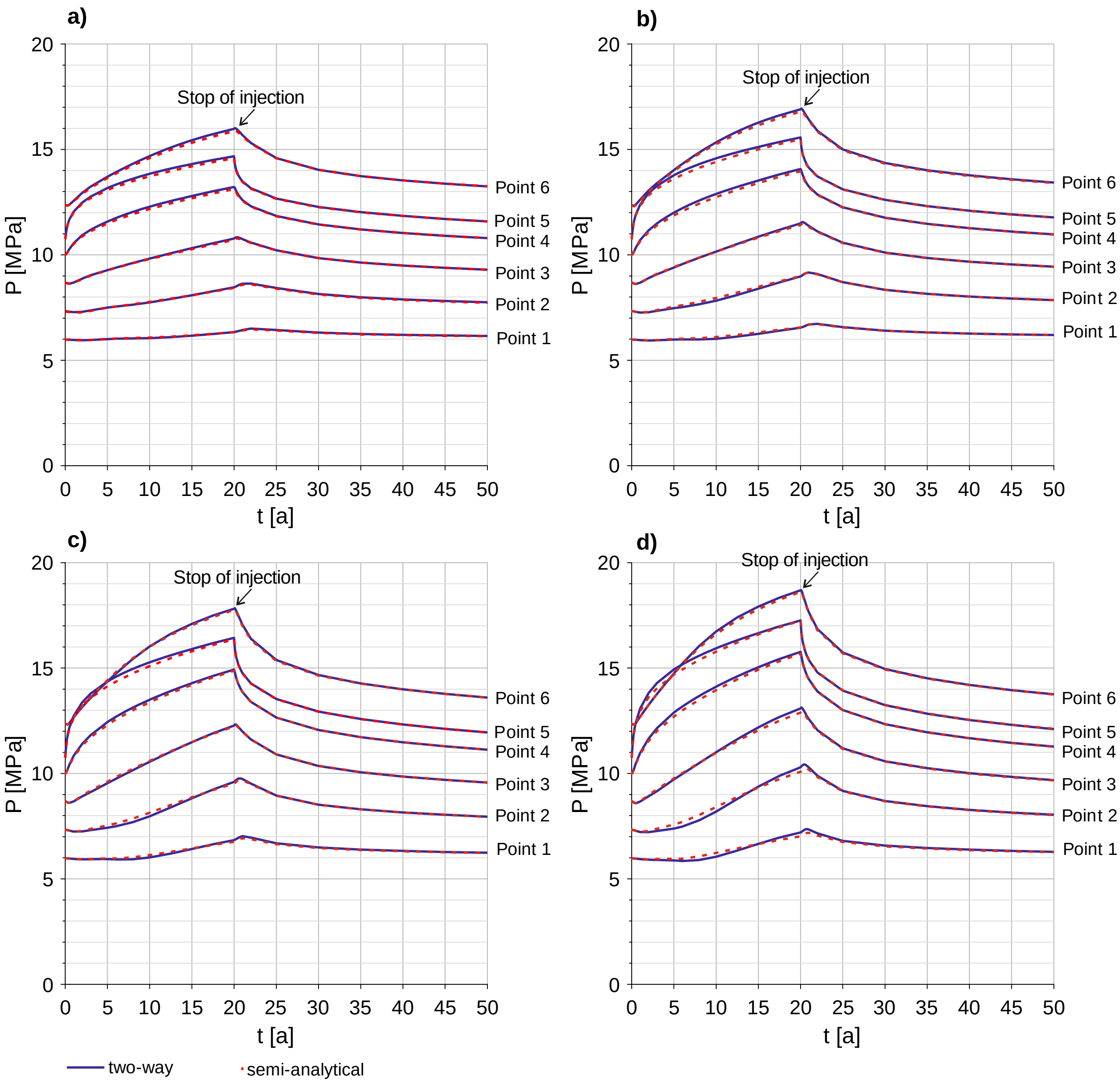

Fig. 8 Pore pressure distribution over time at selected fault depths with $k_{ini}=10^{-16}$ m² and four brine injection rates of a) 0.0018 kg/s/m, b) 0.0023kg/s/m, c) 0.0027 kg/s/m and d) 0.0032 kg/s/m show a very good agreement between the two-way (blue solid line) and semi-analytical coupling schemes (red dashed line).

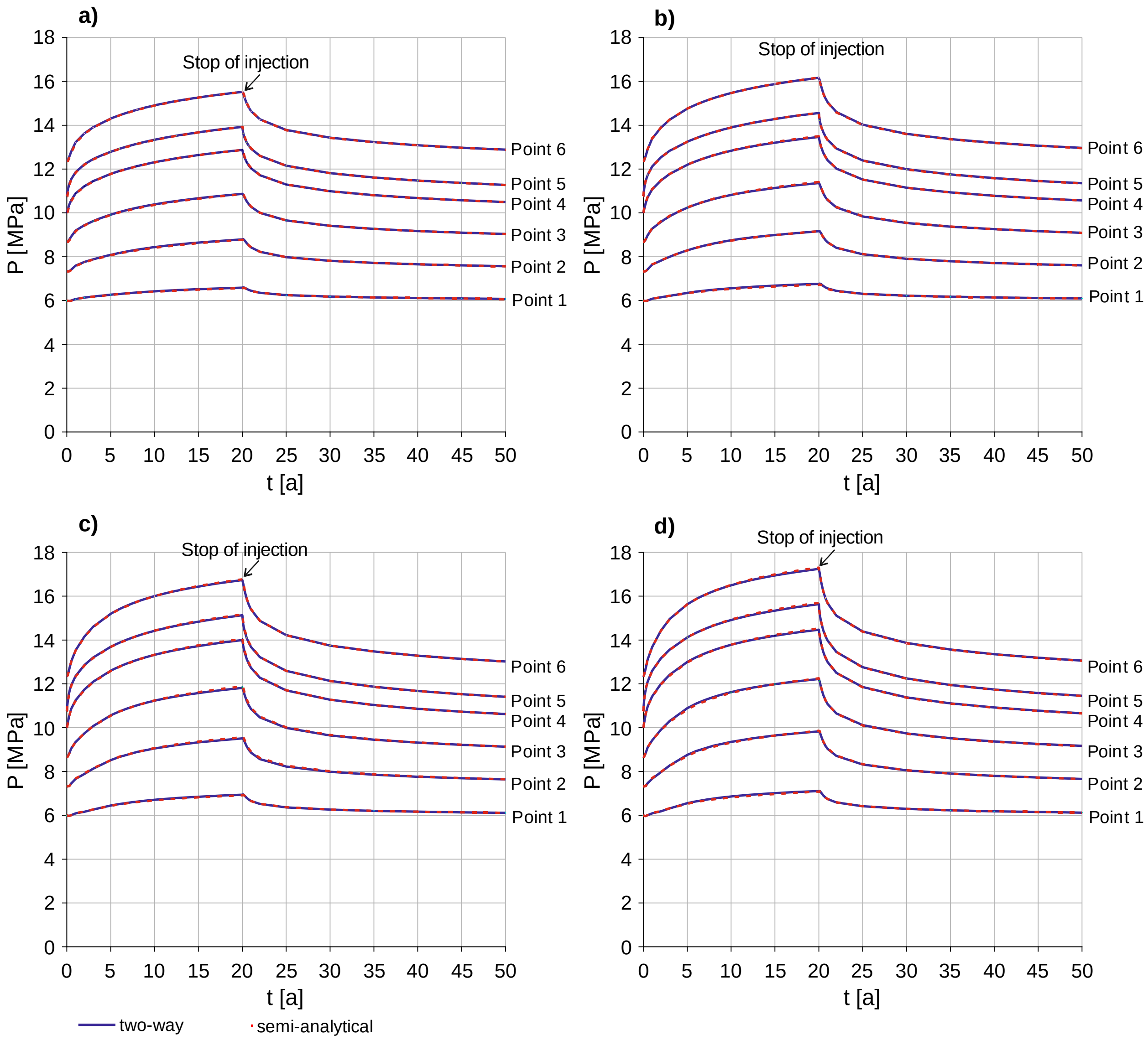

Fig. 9 Pore pressure distribution over time at selected fault depths for $k_{ini}=10^{-15}$ m² and four brine injection rates of a) 0.0018 kg/s/m, b) 0.0023kg/s/m, c) 0.0027 kg/s/m and d) 0.0032 kg/s/m show a very good agreement be-tween the two-way (blue solid line) and semi-analytical coupling schemes (red dashed line).

In the aforementioned simulations, we observe a maximum fault slip of 15.5 cm (simulation S22), accompanied by a maximum pore pressure increase of 7 MPa in the reservoir. These results com-ply qualitatively with the findings of Cappa and Rutqvist (2011). Their investigations of a synthetic model consisting of one single fault zone dipping with 80° show a maximum fault slip of 11.5 cm achieved for a maximum pore pressure increase of approximately 9 MPa. As both investigations use identical material parameters (see Table 4), the results of both studies are comparable and the difference of 4 cm can be explained by the deviation of the dipping angle by 10°.

In Section 3, multiphase fluid flow simulations are used to verify the hypothesis that one set of functions, determined by one base simulation is suitable to significantly reduce the computational time for simulating a multitude of different injection rate scenarios.

3. Application example for fault reactivation due to CO_2 injection considering multiphase fluid flow

The isothermal simulations discussed in the following consider 20-year injection and 30-year post-injection periods. We use the previously discussed one- and two-way hydromechanical coupling approaches by combining the TOUGH2-MP and FLAC^{3D} simulators (Cappa and Rutqvist, 2011; Itasca, 2013; Kempka and Kühn, 2013; Pruess, 2005; Zhang et al., 2008). The applied model parametrization is given in Table 5.

Table 5 Material properties used to simulate CO_2 injection in a reservoir-caprock system with one fault.

Parameters	Reference	Reservoir	Caprock	Underburden	Upper aquifer	Fault
Young's modulus, E (GPa)	Cappa and Rutqvist, 2011	10	10	10	10	1
Poisson's ratio, ν (-)	Cappa and Rutqvist, 2011	0.25	0.25	0.25	0.25	0.25
Rock density, ρ_s (kg/m^3)	Cappa and Rutqvist, 2011	2 260	2 260	2 260	2 260	2 260
Biot's coefficient, α (-)	Cappa and Rutqvist, 2011	1	1	1	1	1
Friction angle, φ (◦)	Cappa and Rutqvist, 2011	-	-	-	-	25
Dilation angle, ψ (◦)	Cappa and Rutqvist, 2011	-	-	-	-	20

Porosity, ϕ (-)	Cappa and Rutqvist, 2011	0.1	-	-	0.1	0.05
Permeability, k (m^2)	Cappa and Rutqvist, 2011	10^{-13}	-	-	10^{-14}	10^{-16}
Residual non-wetting phase (CO_2) saturation (-)	Cappa and Rutqvist, 2011	0.05	-	-	0.05	0.05
Residual wetting phase (water) saturation (-)	assumed	0.15	-	-	0.15	0.15
Capillary entry pressure (van Genuchten 1980)	assumed	12.6	-	-	12.6	12.6
Parameter m (-) (van Genuchten 1980)	assumed	0.65	-	-	0.65	0.65

Beside a reduction of the upper aquifer thickness down to 50 m and an increase of the caprock thickness up to 950 m, a fault width of 40 m as shown in Fig. 10 as well as impermeable caprock and underburden, the model and parameter setup is equal to the one given in Section 2. This adaption was done, as we aim at validating the new approach under extreme conditions, i.e., a doubling of the flow path length through the low permeable part of the fault by increasing the caprock thickness. Considering a hydrostatic pressure gradient and an atmospheric pressure of 0.101325 MPa at the ground surface, the initial fluid pressure at the top of the reservoir equates to 9.91 MPa. The applied injection rates are given in Table 6 and the fault is partitioned into eight element areas here (Points 1 to 8 in Fig. 10) due to the increase of the caprock thickness.

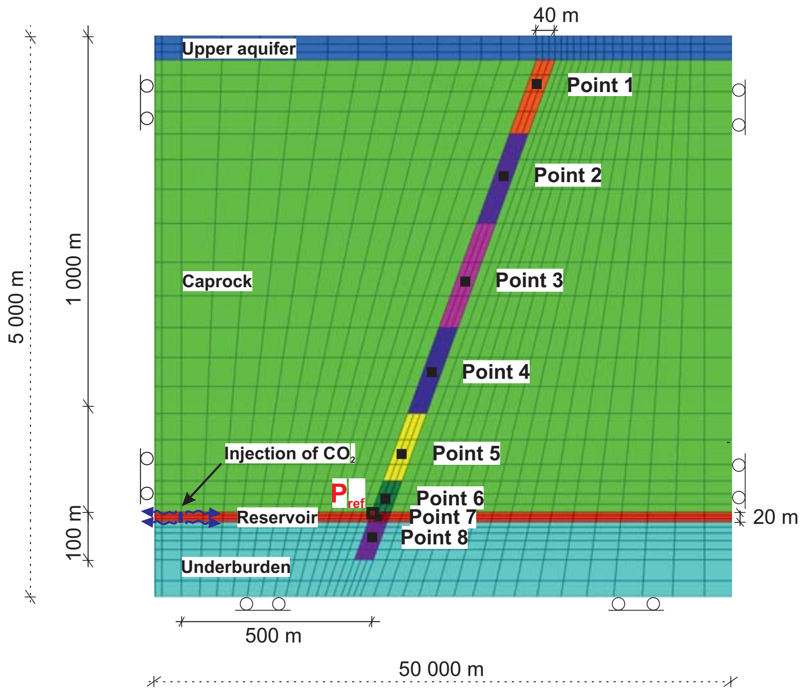

Fig. 10 Close-view of injection elements and fault zone in the synthetic model used for the implementation and validation of the semi-analytical hydromechanical coupling. The black-filled rectangles (Points 1–8) are representative elements and incorporate the hydraulic behavior of the corresponding element group of the fault. The black rectangle at the intersection of the reservoir and the fault is the reference element for the pore pressure P_{Ref}.

To validate the semi-analytical coupling approach for multiphase fluid flow, seven simulations listed in Table 6 are carried out. A one-way coupled single-phase fluid flow base simulation with an initial fault permeability of 5 x 10^{-16} m² (five times higher than in the previously introduced benchmark simulation) and a brine injection rate of 0.0018 kg/s/m determine the base case.

Table 6 Simulations undertaken for validation of the semi-analytical hydromechanical coupling approach by two-way coupled simulations.

Simulation type	Flow phases	Initial fault zone permeability [m²]	Injection rate [kg/s/m]	H-M coupling method
Base case	single	5 x 10^{-16}	0.0018	one-way
Benchmark	multi	1 x 10^{-16}	0.00153	two-way
Benchmark	multi	1 x 10^{-16}	0.0019	two-way
Benchmark	multi	1 x 10^{-16}	0.0023	two-way
Validation	multi	1 x 10^{-16}	0.00153	semi-analytical
Validation	multi	1 x 10^{-16}	0.0019	semi-analytical
Validation	multi	1 x 10^{-16}	0.0023	semi-analytical

Based on this single simulation, the parametrization for the semi-analytical coupling method (see Table 7) used for validation (see Table 6) is determined as previously discussed in Section 2. To assess the obtained results of the innovative coupling, benchmark simulations are undertaken using a sequentially two-way coupled approach according to Table 6.

Table 7 Parametrization of the semi-analytically coupled simulation runs.

		Linearized inclinations of $e(P_{ref})$ functions			Pore pressure control points in the reference cell (P_{ref}) [MPa]	
Point	Depth [m]	α_1 [°]	α_2 [°]	α_3 [°]	$P_{crit\ 1}$	$P_{crit\ 2}$
1	98.9	3.9	0.0	1.0	12.3	12.83
2	290.1	11.7	0.0	2.6	12.44	13.07
3	510.0	15.1	0.0	3.6	12.3	13.34
4	705.2	15.6	0.0	4.1	12.06	13.74
5	873.9	13.8	0.0	4.1	11.77	14.14
6	971.8	11.2	0.4	3.6	11.61	14.38
7	1010.0	9.6	1.9	3.3	11.53	13.97
8	1051.8	7.2	0.4	2.9	11.62	14.52

3.1 Results and discussion

A comparison of pore pressure distributions over time, resulting from three different CO_2 injection rates (see Table 6) using the semi-analytical coupling (red dashed lines) and a two-way coupling (blue solid line) is given in Figures 11 to 13. For the lowest injection rate, the maximum reservoir pore pressure increase is equal to 5.25 MPa, 6.17 MPa for the average one and 7.06 MPa for the highest one. At Point 4, the maximum calculated permeability multipliers (Equations 2 and 3) are 5.7, 7.85 and 12.85, respectively, increasing with the applied injection rate. For all investigated scenarios, we achieve a remarkably good agreement between the validation and benchmark simulation results.

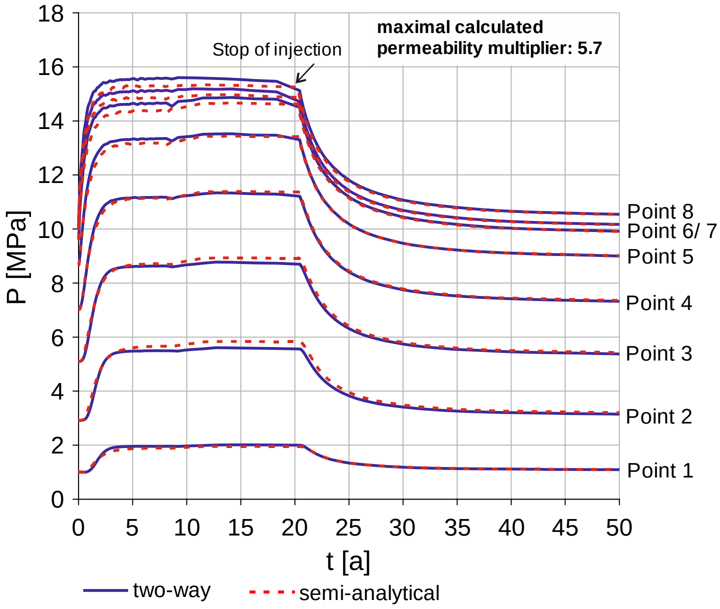

Fig. 11 Pore pressure evolution over time at selected fault depths for $k_{ini}=10^{-16}$ m² and a CO_2 injection rate of 0.00153 kg/s/m shows a very good agreement between the two-way (blue solid line) and semi-analytical coupling (red dashed line). A maximum pore pressure deviation between both coupling methods of 5 % is observed at Point 2.

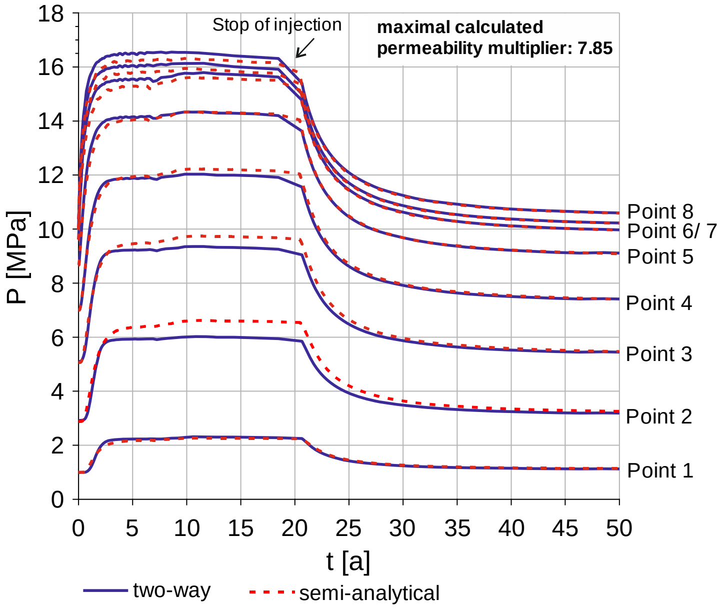

Fig. 12 Pore pressure evolution over time at selected fault depths for $k_{ini}=10^{-16}$ m² and a CO_2 injection rate of 0.0019 kg/s/m shows a very good agreement between the two-way (blue solid line) and semi-analytical coupling (red dashed line). A maximum pore pressure deviation between both coupling methods of 10 % is observed at Point 2.

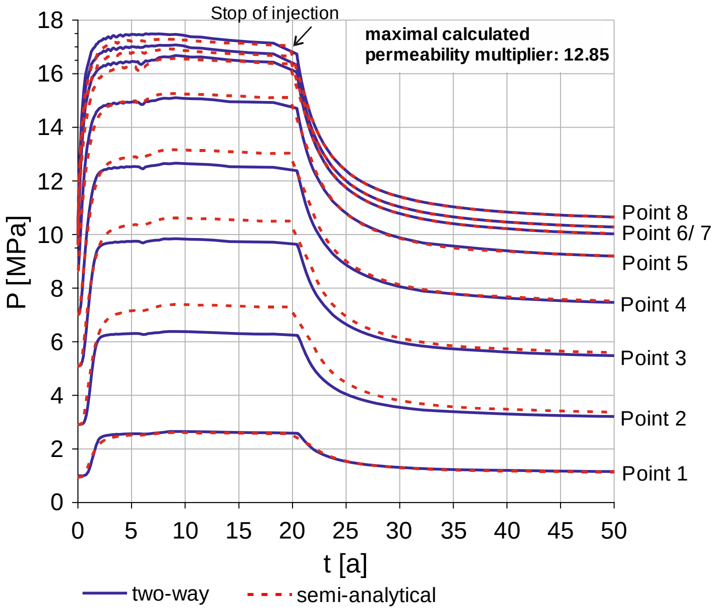

Fig. 13 Pore pressure evolution over time at selected fault depths for $k_{ini}=10^{-16}$ m^2 and a CO_2 injection rate of 0.0023 kg/s/m shows a good agreement for the two-way (blue solid line) and semi-analytical coupling (red dashed line). A maximum pore pressure deviation between both coupling methods of 20 % is observed at Point 2.

Even under this extreme model setup, considering a caprock thickness of 950 m not intersected by aquifers draining the fault, only minor deviations between both coupling approaches are observed at Points 2, 3 and 4. In Fig. 11, representing the pore pressure distributions for the lowest injection rate, we observe a deviation of approximately 5 %, in Fig. 12 one of 10 % and in Fig. 13 one of 20 % for the highest injection rate. Anyhow, compared to the results given in Section 2, we observe higher deviations in pore pressure distribution over time between both coupling approaches. This can be explained by an increase in nonlinearity of the void ratio evolution, induced by the increased flow path length of the fault zone.

The required computational time of the semi-analytical coupling approach is significantly lower than that of the sequential two-way coupling, what emphasizes the actual benefit of using this innovative coupling method. While the semi-analytical coupling needs between 1.5 and 2.5 hours CPU time using a parallel calculation on four AMD Opteron 6320 processors (TOUGH2-MP), the two-way coupled computation consumes between 21.5 and 38.0 hours on one Intel E5-2687W

CPU (FLAC^{3D}) and four AMD Opteron 6320 processors (TOUGH2-MP). Savings in computational time by a factor of up to 15 enable carrying out a multitude of time-consuming multiphase fluid flow simulations coupled with mechanics as applied in probabilistic assessments such as uncertainty and risk analyses.

4. Conclusions

The comparative study discussed at the beginning of this manuscript introduces a new computationally-efficient semi-analytical hydromechanical coupling approach for fault reactivation and demonstrates its theoretical validity. In this context, fault reactivation is determined by the Mohr-Coulomb failure criterion and ideal-elastic material behavior, controlled by the fault's friction and dilatancy. Even though this approach may not accurately represent the complex geological reality, it allows to carry out coupled numerical assessments on fault reactivation at reservoir to regional scale. For that purpose, we assumed relatively simple material behaviour, avoiding potential superposition effects that could have limited the portability of the numerical findings into semi-analytical transfer functions.

Based on linearized $e(P_{ref})$ functions at representative fault depths, derived by a one-way coupled single phase fluid flow base simulation, we defined analytical functions which are directly implemented into a hydraulic simulator to update the fault's porosity and permeability. As a one-way coupling shows a linear relation between the void ratio and a reference pore pressure P_{ref}, we demonstrated how these functions can be easily parametrized by three inclinations α_1, α_2 and α_3 and two control pore pressures $P_{crit\,1}$ and $P_{crit\,2}$. Furthermore, we demonstrated that aside from $P_{crit\,2}$ this parametrization is injection rate-independent and different initial fault permeabilities result in a shift of the analytical functions controlled by $P_{crit\,1}$, only.

Subsequently, we presented that a sufficient approximation of the nonlinear void ratio-over-reference pore pressure behavior, obtained by two-way coupled simulations can be achieved by the semi-analytical approach considering a parametrization based on the $e(P_{ref})$ function of a single one-way coupled base simulation. For that purpose, we demonstrated that using a fault permeability multiplier of five is appropriate in the base case simulation, while, the semi-analytically coupled simulations do not consider a specific multiplier, and thus the initial fault permeability.

Finally, we validated the semi-analytical hydromechanical coupling approach for hydraulic reactivation of fault zones for multiphase fluid flow simulations. Using a multiphase fluid flow simulator coupled to a geomechanical simulator at 2D plane-strain conditions, the hydraulic reactivation of a fault zone induced by CO_2 injection into a saline aquifer was simulated. Our approach was then validated by comparison against sequentially two-way coupled simulation results. In this context, the semi-analytical coupling scheme exhibits a remarkably good agreement with pore pressure distributions even under extreme conditions, i.e., low initial permeabilities and relatively long flow path lengths along the fault due to the 950-m caprock thickness not intersected by intermediate aquifers in our synthetic model, resulting in a significant reduction of the required computational time by a factor of up to 15.

This gain in computational time allows for the application of two-way coupled hydromechanical simulations, incorporating multiphase fluid flow in a more efficient way and contributes to the implementation of probabilistic assessments as required for uncertainty and risk analyses. Consequently, a high number of realizations to assess all relevant parameter uncertainties can be undertaken with the support of this innovative coupling approach.

To avoid exceeding the purpose of the present study as well as for the sake of comprehensibility, the determination of the new semi-analytical coupling approach has been undertaken assuming exclusively the Mohr-Coulomb failure criterion. As this failure criterion is only one besides many others, our further research will specifically test our coupling approach against other fault failure modes, i.e., a stick-slip mode or a ubiquitous joint model. Therefore, different constitutive models have to be applied in the geomechanical simulator and the parametrization of our semi-analytical coupling approach has to be adapted in an appropriate manner. In the next step, we aim to validate our semi-analytical coupling approach in 3D.

Acknowledgements

The authors gratefully acknowledge the funding support from the German Federal Ministry of Education and Research. The present study was undertaken in the frame of the BMBF/DFG GE-OTECHNOLOGIEN program (Grant 03G0760A/D). Furthermore, we would like to express our gratitude to the CO_2RINA project partners for data provision and scientific discussions.

References

ABAQUS. 2010. Unified Finite Element Analysis. User's Manual Version 6.10. 2010. Providence, Rohde Island, USA: Dassault Systèmes. Simulia Corporation.

Adams, M., Feinendegen, M., Tillner, E., Kempka, T., Ziegler, M. 2015. Geologische CO_2-Speicherung: Vergleich unterschiedlicher Kopplungsansätze für die hydraulische Reaktivierung von Störzonen. In: 2. Deutsche Bodenmechanik Tagung: Bochum, 19.5.2015 / Hrsg.: Deutsche Gesellschaft für Geotechnik e.V., Essen, DGGT, ISBN: 978-3-662-45990-4 [in German].

Altmann, J.B., Müller, B.I.R., Müller, T.M., Heidbach, O., Tingay, M.R.P., Weißhardt, A., 2014. Pore pressure stress coupling in 3D and consequences for reservoir stress states and fault reactivation. Geothermics, 52:195-205.

Battistelli, A. C. Calore and K. Pruess, 1997. The Simulator TOUGH2/EWASG for Modeling Geothermal Reservoirs with Brines and Non-Condensible Gas. Geothermics, 26(4):437-464.

Birkholzer, J.T., Zhou, Q., Tsang, C.-F. (2009): Large-scale impact of CO_2 storage in deep saline aquifers: A sensitivity study on pressure response in stratified systems. International Journal of Greenhouse Gas Control, 3:181-194.

Cappa, F., Rutqvist, J. 2011. Modeling of coupled deformation and permeability evolution during fault reactivation induced by deep underground injection of CO_2. International Journal of Greenhouse Gas Control, 5:336-346.

Chabab E., Kempka T. 2016. Quantification of fluid migration via faults requires two-way coupled hydromechanical simulations. Energy Procedia, 97:372-378.

Chin, L.Y., Raghavan, R., Thomas, L.K. 2000. Fully coupled geomechanics and fluid flow analysis of wells with stress-dependent permeability. SPE J, 5(1):32–45, Paper 58968.

Holloway, S. 2005. Underground sequestration of carbon dioxide – a viable greenhouse gas mitigation option. Energy, 30, S. 2318-2333.

IPCC 2005. IPCC Special Report on Carbon Dioxide Capture and Storage. Prepared by Working Group III of the Intergovernmental Panel on Climate Change, Cambridge University Press, Cambridge, United Kingdom and New York, NY, USA.

Itasca. 2013. $FLAC^{3D}$ – Fast Lagrangian Analysis of Continua in 3 Dimensions. User's Manual.

Kempka, T., Kühn, M. 2013. Numerical simulations of CO_2 arrival times and reservoir pressure coincide with observations from the Ketzin pilot site, Germany. Environmental Earth Science, 70(8):3675-3685.

Kempka, T., Klapperer, S. 2014. and Norden, B.: Coupled hydromechanical simulations demonstrate system integrity at the Ketzin pilot site for CO_2 storage, in: Rock Engineering and Rock

Mechanics: Structures in and on Rock Masses; Proceedings of EUROCK 2014, ISRM European Regional Symposium, edited by: Alejano, L., Perucho, A., Olalla, C., and Jiménez, R., Leiden: CRC Press/Balkema, 1317–1322.

Kempka, T., Nielsen, C.M., Frykman, P., Shi, J.Q., Bacci, G., Dalhoff, F. 2015. Coupled Hydro-Mechanical Simulations of CO_2 Storage Supported by Pressure Management Demonstrate Synergy Benefits from Simultaneous Formation Fluid Extraction. Oil & Gas Science and Technology, 70(4):599–613.

Langhi, L., Zhang, Y., Gartrell, A., Underschultz, J., Dewhurst, D. 2010. Evaluating hydrocarbon trap integrity during fault reactivation using geomechanical three-dimensional modeling: An example from the Timor Sea, Australia. AAPG Bulletin, 94(4):567–591.

Lautenschläger, C.E.R., Righetto, G.L., Inoue, N., Fontoura, S.A.B. 2013. Advances on Partial Coupling in Reservoir Simulation: A New Scheme of Hydromechanical Coupling. 2013 North Africa Technical Conference & Exhibition. SPE Paper Number 164657.

Mandl, G. 1988. Mechanics of tectonic faulting – models and basic concepts. Developments in Structural Geology 1, ed. H.J. Zwart, Elsevier.

Nguyen, B.N., Hou, Z., Last, G.V., Bacon, D.H. 2016. Three-dimensional analysis of a faulted CO2 reservoir using an Eshelby-Mori-Tanka approach to rock elastic properties and fault permeability. Journal of Rock Mechanics and Geotechnical Engineering, 8:828-845.

Orlic, B. 2016. Geomechanical effects of CO_2 storage in depleted gas reservoirs in the Netherlands: Inferences from feasibility studies and comparison with aquifer storage. Journal of Rock Mechanics and Geotechnical Engineering, 8:846-859.

Pan, P., Wu, Z., Feng, X., Yan, F. 2016. Geomechanical modeling of CO_2 geological storage: A review. Journal of Rock Mechanics and Geotechnical Engineering, 8:936-947.

Pruess, K. 2005. ECO2N: A TOUGH2 Fluid Property Module for Mixtures of Water, NaCl, and CO_2. Report LBNL-57952, Lawrence Berkeley National Laboratory, Berkeley, California.

Righetto, G.L., Lautenschläger, C.E.R., Inoue,N., Fontoura, S.A.B. 2013. Analysis of the hydromechanical behavior of fault zones in petroleum reservoirs. EUROCK 2013 – The 2013 ISRM International Symposium.

Rutqvist, J. & Tsang, C.-F., 2002. A study of caprock hydromechanical changes associated with CO_2 injection into a brine aquifer. Environ. Geol. 42, 296–305.

Rutqvist, J., Birkholzer, J., Cappa, F., Tsang, C.F. 2007. Estimating maximum sustainable injection pressure during geological sequestration of CO_2 using coupled fluid flow and geomechanical fault-slip analysis. Energy Conversion and Management, 48:1798–1807.

Rutqvist, J., Birkholzer, J., Tsang, C.F. 2008. Coupled reservoir geomechanical analysis of the potential for tensile and shear failure associated with CO_2 injection in multilayered reservoir–caprock systems. International Journal of Rock Mechanics and Mining Sciences, 45:132–143.

Rutqvist, J. 2010. Coupled reservoir-geomechanical analysis of CO_2 injection and ground deformations at In Salah, Algeria. International Journal of Greenhouse Gas Control, 4:225–230.

Rutqvist, J., Rinaldi, A.P., Cappa, F., Jeanne, P., Mazzoldi, A., Urpi, L., Guglielmi, Y., Vilarrasa, V. 2016. Fault activation and induced seismicity in geological carbon storage – Lessons learned from recent modeling studies. Journal of Rock Mechanics and Geotechnical Engineering, 8:789-804.

Settari, A., Mourits, M. 1994. Coupling of geomechanics and reservoir simulation models. In Computer Methods and Advances in Geomechanics. pp. 2151-2158. Siriwardane & Zanan (eds.), Balkema, Rotterdam.

Settari A., Bachman, R.C., Walters, D.A. 2005. How to approximate effects of geomechanics in conventional reservoir simulation. SPE Annual Technical Conference and Exhibition. SPE Paper Number 97155-MS.

Settari A. 2012. Workflow for coupled geomechanical and reservoir problems – recent experiences. 74th EAGE Conference & Exhibition incorporating SPE EUROPEC 2012.

Spycher, N., Pruess, K., Ennis-King, J. 2003. CO_2-H_2O Mixtures in the Geological Sequestration of CO_2. I. Assessment and Calculation of Mutual Solubilities from 12 to 100°C and up to 600 bar. Geochimica et Cosmochimica. Acta, 67(16):3015.

Tillner, E., Kempka, T., Nakaten, B., Kühn, M. 2013. Brine migration through fault zones: 3D numerical simulations for a prospective CO_2 storage site in Northeast Germany. International Journal of Greenhouse Gas Control, 19: 689-703.

Tillner, E., Shi, J.Q., Bacci, G., Nielsen, C.M., Frykman, P., Dalhoff, F., Kempka, T. 2014. Coupled Dynamic Flow and Geomechanical Simulations for an Integrated Assessment of CO_2 Storage Impacts in a Saline Aquifer. Energy Procedia, 63:2879–2893.

Van Genuchten, M.Th. 1980. A closed-form equation for predicting the hydraulic conductivity of unsaturated soils. Soil Science Society of America J, 44(5):892-898.

Verdon, J.P., Stork, A.L. 2016. Carbon Capture and Storage, geomechanics and induced seismic activity. Journal of Rock Mechanics and Geotechnical Engineering, 8:928-935.

Vilarrasa, V., Makhnenko, R., Gheibi, S. 2016. Geomechanical analysis of the influene of CO_2 injection location on fault stability. Journal of Rock Mechanics and Geotechnical Engineering, 8:805-818.

Walters, D.A., Settari, A., Kry, R.P. 2002. Coupled geomechanical and reservoir modeling investigating poroelastic effects of cyclic steam stimulation in the cold lake reservoir. SPE Reservoir Evaluation & Engineering 5(2):507-516. SPE Paper Number 80997-PA.

Zhang, K., Wu, Y.S., Pruess, K. 2008. User's Guide for TOUGH2-MP – A Massively Parallel Version of the TOUGH2 Code. Report LBNL-315E, Earth Sciences Division, Lawrence Berkeley National Laboratory, Berkeley, California.

Zhang, Y., Gartrell, A., Undershultz, J.R., Dewhurst, D.N. 2009. Numerical modelling of strain localisation and fluid flow during extensional fault reactivation: Implcations for hydrocarbon preservation. Journal of Structural Geology 31 (2009):315-327.

Zhang, Y., Roberts, P.A., Murphy, B. 2010. Understanding regional structural controls on mineralization at the century deposit: A numerical modelling approach. Journal of Geochemical Exploration 106 (2010):244-250.

Zhang, Y., Underschultz, J.R., Gartrell, A., Dewhurst, D.N., Langhi, L. 2011. Effects of regional fluid pressure gradients on strain localisation and fluid flow during fault reactivation. Marine and Petroleum Geology, 28:1703-1713.

Zhang, Y., Schaubs, P.M., Sheldon, A., Poulet, T., Karrech, A. 2013. Modelling fault reactivation and fluid flow around a fault restraining step-over structure in the Laverton gold region, Yilgarn Craton, Western Australia. Geofluids (2013), 13:127-139.

Zhang, Y., Langhi, L., Schaubs, P.M., Piane, C.D., Dewhurst, D.N., Stalker, L., Michael, K. 2015. Geomechanical stability of CO2 containment at the South West Hub Western Australia: a coupled geomechanical-fluid flow modelling approach. International Journal of Greenhouse Gas Control. Vol. 37:12-23.